

Laser Doppler Spectroscopy in an Oscillating Electric Field

Alan J. Bennett and E. E. Uzgiris

General Electric Research and Development Center, Schenectady, New York 12301

(Received 10 May 1973)

We investigate the photocurrent power spectrum induced by laser light scattered to a detector from a suspension of homogeneous charged particles in the presence of a square-wave electric field. Constraints associated with optimal heat dissipation require that a time-dependent field be used in order to obtain good resolution in measurements of electrophoretic mobilities. A calculation of the power spectrum yields an expression that depends on both the diffusion constant and electrophoretic mobility of the particle. This expression is used to analyze experimental data in order to obtain values for those parameters.

I. INTRODUCTION

The broadening of the spectrum of light scattered from randomly moving particles is a well-known effect and has been extensively used in recent years for the measurement of diffusion constants by the technique of light-beating spectroscopy.^{1,2} The technique has proven to be extremely rapid, highly accurate, and highly sensitive.³ Extensions of the technique for the measurement of the characteristics of particles undergoing directed motion retain these happy features and allow the determination of not only diffusion constants but also of electrophoretic mobilities.⁴⁻⁶ In principle, with a suitable electric field and heterodyne detection, it is possible to determine the instantaneous electrophoretic velocity from the spectral characteristics of the scattered light.

Unlike the classical methods of electrophoresis⁷ which make use of a constant electric field, the laser-light-scattering methods used heretofore require a time-varying electric field in order to obtain high resolution. The difference is, in large part, due to the fact that in the classical methods one essentially measures a displacement, whereas in the light-scattering methods one measures instantaneous velocity. Thus resolution is increased in the former methods by waiting a longer period of time or increasing the applied electric field, but in the latter method only by operating as higher electric fields can one increase the velocity separations of the constituents under study. Unfortunately, when high electric fields are applied across a conducting solution all or some of the following deleterious effects may occur: convective instabilities due to Joule heating, electrode reactions with gas bubbling, electrode polarization effects, and concentration gradient effects. Application of a pulsed or oscillating square-wave electric field rather than a dc electric field minimizes these effects and

allows the attainment of high-resolution Doppler spectra. In addition, with a square-wave field there is no transit-time broadening, i.e., there is no frequency uncertainty arising from the finite time of traversal across the laser beam.

Ware and Flygare used a pulsed electric field to measure the electrophoretic mobilities of bovine serum albumin⁴ and fibrinogen⁶ in a scattering cell very much like the Tiselius electrophoresis cell.⁷ They applied alternating polarity voltage pulses (of 0.1-sec duration and spaced about 1 sec apart) to electrodes separated by about 10 cm. This low-duty-cycle pulse technique avoids convective turbulence from Joule heating but results in rather inefficient spectral data collection and requires gated signal analysis. Furthermore, if the pulse length is made short (less than 0.1 sec, for example) as it must be if a high electric field is applied to the conducting solution, then artificial broadening of the Doppler spectra can become significant. Nevertheless, Ware and Flygare were able to make accurate mobility determinations for the proteins investigated and resolve spectral components for a mixture of such proteins.

The square-wave electric field technique considered here (Fig. 1) requires relatively simple electronics and, more importantly, results in perfect spectral-data-collection efficiency. Broadening of the Doppler spectra from the application of a finite length pulse is also avoided by this technique. In our experiments, turbulence from convective instabilities is minimized by use of a narrow-gap electrode arrangement which avoids large temperature gradients in the scattering region of the cuvette.

In some cases for which the random motions are fast compared to the frequency of electric field reversal, the electric field may be regarded as quasistationary. In general, however, the switching introduces added structure in the power spec-

trum of the scattered light. Spectral peaks occur at the harmonics of the switching frequency and the interpretation of the spectra is not straightforward. It is the purpose of this paper to describe and interpret the Doppler spectra which results from the scattering of light from particles subjected to a square-wave electric field. It will be shown below that the spectral resolution obtained in an oscillating field is equivalent to the spectral resolution obtained in a dc electric field. Therefore, the accuracy of the mobility measurement should, in principle, be comparable to the accuracy obtainable from an ideal system in which the electric field is kept constant.

In Sec. II, we review the standard calculation of the heterodyne power spectrum obtained in the presence of a dc field. We then extend that treatment to the case of the square wave. Section III contains a brief description of the experimental apparatus. The results of Sec. II are then used to analyze the data obtained and assess the usefulness of our approach. Some concluding remarks constitute Sec. IV.

II. CALCULATION

A. Review of Heterodyne Detection Formalism

In a heterodyne mixing spectrometer,^{1,2} the total field incident on the photosurface is given by

$$E_T(\mathbf{r}, t) = E_0(\mathbf{r})e^{-i\omega t} + E_s(\mathbf{r}, t). \quad (2.1)$$

The first term is due to the local oscillator and the second to the scattered light.

The photocurrent is

$$i(t) = \alpha \int |E_T(\mathbf{r}, t)|^2 dA, \quad (2.2)$$

where

$$\alpha = (Ge\eta/h\nu)(c/8\pi) \quad (2.3)$$

with G the photodetector gain, e the electron charge, η the quantum efficiency, c the speed of light, $h\nu$ the light quantum energy, and dA a differential detector area.

For simplicity, it is assumed that both E_0 and E_s are in phase over the detector surface A . Then for $E_0 \gg E_s$ the photocurrent autocorrelation function is given approximately by

$$\begin{aligned} R_i(t, \tau) &= \langle i(t)i(t+\tau) \rangle \\ &= 2\alpha i_0 A \operatorname{Re} \langle e^{i\omega\tau} E_s(t+\tau) E_s^*(t) \rangle \\ &= 2\alpha i_0 A \operatorname{Re} R_E(t, \tau), \end{aligned} \quad (2.4)$$

where $\langle \rangle$ represents an ensemble average,

$$i_0 = \alpha |E_0|^2 A,$$

and here, and in what follows, dc and shot-noise

terms are not included. The scattered-field autocorrelation function $R_E(t, \tau)$ may be evaluated by setting

$$E_0(\mathbf{r}) = \mathcal{E}_0 e^{i\mathbf{k}_0 \cdot \mathbf{r}} \quad (2.5)$$

and

$$E_s(\mathbf{r}, t) = \mathcal{E}_s e^{-i\omega t} \sum_{j=1}^N e^{i\varphi_j(t)}. \quad (2.6)$$

Here \mathcal{E}_s is the amplitude of the field scattered by each of the N particles in the solution in which an origin of coordinates is taken to be a distance R from the detector and

$$\mathcal{E}_s = \mathcal{E}_0 [e^{i\mathbf{k}_s \cdot \mathbf{R}} / R] (\omega/c)^2 (\alpha - \alpha_0) V \sin\Phi, \quad (2.7)$$

where \mathbf{k}_s is the wave vector of the scattered wave, Φ is the angle between the direction of polarization of \mathbf{E}_0 and \mathbf{k}_s , $\alpha - \alpha_0$ is the difference between the dipole polarizability of the particle and the solvent and V is the particle volume. The phase factor $\varphi_j(t)$ for a given scatterer is the path length from an incident to a scattered wave front relative to an origin in the scattering volume.¹ Thus

$$\varphi_j(t) = (\mathbf{k}_0 - \mathbf{k}_s) \cdot \mathbf{r}_j(t) = \mathbf{K} \cdot \mathbf{r}_j(t), \quad (2.8)$$

with

$$K = \frac{4\pi}{\lambda/n} \sin \frac{1}{2}\theta,$$

where $\mathbf{r}_j(t)$ is the vector between the origin of coordinates in the solution and the particles, n is the solvent index of refraction, and θ is the angle between \mathbf{k}_0 and \mathbf{k}_s . Substituting (2.6) and (2.8) into the field autocorrelation function, one obtains

$$R_E(t, \tau) = |\mathcal{E}_s|^2 \left\langle \sum_{ij} e^{i\mathbf{K} \cdot [\mathbf{r}_i(t+\tau) - \mathbf{r}_j(t)]} \right\rangle. \quad (2.9)$$

For uncorrelated motion, only terms with $i=j$ are nonzero. After ensemble averaging, since each particle is taken to be equivalent and spherical, one has

$$R_i(t, \tau) = 2\alpha i_0 AN |\mathcal{E}_s|^2 \operatorname{Re} \langle e^{i\mathbf{K} \cdot [\mathbf{r}(t+\tau) - \mathbf{r}(t)]} \rangle. \quad (2.10)$$

For a homogeneous isotropic stationary system,

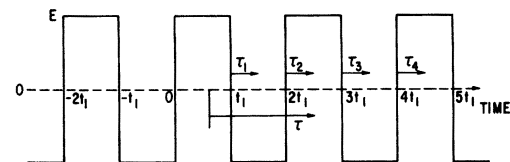


FIG. 1. The experimental electric field vs time. The temporal variables used in Sec. II are defined in the figure.

the phase-correlation function can be written explicitly as

$$R_{\vec{r}}(t, \tau) = \langle e^{i\vec{k} \cdot [\vec{r}(t+\tau) - \vec{r}(t)]} \rangle = \int W(R, \tau) e^{i\vec{k} \cdot \vec{R}} d^3R, \quad (2.11)$$

where $W(R, \tau)$ is the conditional probability that a particle centered at r at time t will be $r+R$ at time $t+\tau$. This probability satisfies the equation

$$\frac{\partial W}{\partial t} = D\nabla^2 W + \mu E_x \frac{\partial W}{\partial x}, \quad (2.12)$$

where the first term accounts for diffusion and the second for the possible presence of a uniform field E_x . Here μ is the electrophoretic mobility of the particle.

As is well known,⁸ the power spectrum associated with the observed current may be related to its autocorrelation function. In general

$$G(\nu) = \lim_{T \rightarrow \infty} 2 \int_{-\infty}^{\infty} e^{-i\nu\tau} \left(\frac{1}{2T} \int_{-T}^T R_i(t, \tau) dt \right) d\tau, \quad (2.13)$$

where $\nu = \omega/2\pi$. For a stationary process, in which R_i is independent of t , this reduces to the Wiener-Khinchin formula

$$G(\nu) = 2 \int_{-\infty}^{\infty} R_i(\tau) e^{-i\nu\tau} d\tau. \quad (2.14)$$

B. dc Applied Field

For a constant applied field in the x direction, the solution to (2.12) may be obtained by Fourier analysis as

$$W(\vec{r}, \tau) = (4\pi D\tau)^{-3/2} \exp - \left\{ \left[(x + \mu E\tau)^2 + y^2 + z^2 \right] / 4D\tau \right\}. \quad (2.15)$$

Substituting this into Eqs. (2.11) and (2.10):

$$R_i(t, \tau) \equiv R_i(\tau) = \beta e^{-\gamma\tau} \cos(\Omega\tau), \quad (2.16)$$

where

$$\beta = 2\alpha i_0 AN |\mathcal{G}_s|^2, \quad (2.17)$$

$$\gamma = K^2 D, \quad (2.18)$$

$$\begin{aligned} R_i(t, \tau) &= \beta e^{-\gamma\tau} \cos[\Omega\tau], & t_1 - t > \tau > 0, \\ &= \beta e^{-\gamma\tau} \cos[\Omega(t_1 - t) - \Omega\tau_1], & (t_1 - t) + t_1 > \tau > t_1 - t, \\ &= \beta e^{-\gamma\tau} \cos[\Omega(t_1 - t) - \Omega t_1 + \Omega\tau_2], & (t_1 - t) + 2t_1 > \tau > (t_1 - t) + t_1, \end{aligned} \quad (2.24)$$

etc., where

$$\tau_1 = \tau - (t_1 - t), \quad \tau_2 = \tau - [(t_1 - t) + t_1]. \quad (2.25)$$

The sign of the τ_i -dependent terms in the cosine arguments varies in successive intervals due to the change in sign of the electric field. The phase memory is, however, retained. For $0 < t < t_1$ and $\tau > 0$, the general expression for the correlation function can be written,

$$\Omega = \mu EK_x. \quad (2.19)$$

For this stationary case, the power spectrum is given by Eq. (2.14) as

$$G(\nu) = 2\beta\gamma \left(\frac{1}{\gamma^2 + (\omega - \Omega)^2} + \frac{1}{\gamma^2 + (\omega + \Omega)^2} \right). \quad (2.20)$$

Since $G(\omega)$ is symmetric about $\omega = 0$, positive and negative parts can be combined to yield the positive frequency spectrum

$$G^+(\nu) = \frac{4\beta\gamma}{\gamma^2 + (\omega - \Omega)^2}. \quad (2.21)$$

C. ac Applied Field

We now consider the power spectrum associated with the type of applied field used in our experimental work. We use the square wave of frequency $\nu_M = 1/(2t_1)$ which is shown in Fig. 1. The photocurrent correlation function $R_i(t, \tau)$ is no longer stationary and Eq. (2.13) must be used to obtain the power spectrum.

Since the alternating field is applied for very many cycles, it is clear that the integral over t is equivalent to an integral over the interval $0 < t < 2t_1$. In fact, integration over the interval $0 < t < t_1$ is sufficient by the obvious symmetry arguments or by the specific results that follow. The power spectrum Eq. (2.13) can be written as

$$\begin{aligned} G(\nu) &= \frac{2}{t_1} \int_0^{t_1} \int_0^{\infty} R_i(t, \tau) e^{-i\nu\tau} d\tau dt \\ &+ \frac{2}{t_1} \int_0^{t_1} \int_{-\infty}^0 R_i(t, \tau) e^{-i\nu\tau} d\tau dt. \end{aligned} \quad (2.22)$$

Again either a symmetry argument or specific calculation indicates that the second term equals the complex conjugate of the first. Thus

$$G(\nu) = \frac{4}{t_1} \text{Re} \left(\int_0^{t_1} \int_0^{\infty} R_i(t, \tau) e^{-i\nu\tau} d\tau dt \right). \quad (2.23)$$

For $0 < t < t_1$ and $\tau > 0$, the correlation function may be written, with the use of Eq. (2.16), as

$$\begin{aligned}
R_j(t, \tau) &= \beta e^{-\gamma \tau} \cos \Omega \tau, & t_1 - t > \tau > 0; \\
&= \beta e^{-\gamma \tau} \cos[\Omega(t_1 - t - \tau_{j-1})], & j=2, 4, 6, \dots \\
&= \beta e^{-\gamma \tau} \cos[\Omega(-t + \tau_{j-1})], & j=3, 5, 7, \dots
\end{aligned} \tag{2.26}$$

for

$$-t + jt_1 > \tau > -t + (j-1)t_1.$$

Here

$$\tau_j = \tau - jt_1 + t. \tag{2.27}$$

These expressions may now be used in Eq. (2.23) to yield

$$G(\nu) = \frac{4\beta}{t_1} \operatorname{Re} \left\{ \int_0^{t_1} \int_0^{t_1-t} e^{-(\gamma+i\omega)\tau} \cos \Omega \tau \, d\tau \, dt + \sum_{j=2}^{\infty} \int_0^{t_1} \int_{-t+(j-1)t_1}^{-t+jt_1} e^{-(\gamma+i\omega)\tau} \begin{bmatrix} \cos \Omega(t_1 - t - \tau_{j-1}) \\ \cos \Omega(-t + \tau_{j-1}) \end{bmatrix} \right\} d\tau \, dt, \tag{2.28}$$

where the upper and lower cosines are used in even and odd j terms, respectively. This expression is, as noted above, independent of the sign of Ω (and hence E). If, in the second term, we change the τ variable of integration to $x \equiv \tau_{j-1}$, using

$$\tau = x - t + (j-1)t_1 \tag{2.29}$$

and combine successive even and odd j terms in the sum, we can rewrite Eq. (2.28) as

$$G(\nu) = \frac{4\beta}{t_1} \operatorname{Re} \left(I + \sum_{j=2,4,\dots} \alpha_j II \right), \tag{2.30}$$

with

$$I = \int_0^{t_1} \int_0^{t_1-t} e^{-(\gamma+i\omega)\tau} \cos \Omega \tau \, d\tau \, dt, \tag{2.31}$$

$$\alpha_j = e^{-(\gamma+i\omega)(j-1)t_1}, \tag{2.32}$$

$$II = \int_0^{t_1} dt \left(e^{(\gamma+i\omega)t} + e^{-(\gamma+i\omega)t} \right) \int_0^{t_1} dx e^{-(\gamma+i\omega)x} \cos[\Omega(t_1 - t - x)]. \tag{2.33}$$

We now evaluate these expressions. The sum

$$S = \sum_{j=2,4,\dots} \alpha_j = e^{(\gamma+i\omega)t_1} \sum_{j=2,4,\dots} e^{-(\gamma+i\omega)t_1 j} = \frac{1}{2 \sinh[(\gamma+i\omega)t_1]} = \frac{(\sinh \gamma t_1 \cos \omega t_1) - i(\cosh \gamma t_1 \sin \omega t_1)}{\cosh 2\gamma t_1 - \cos 2\omega t_1}. \tag{2.34}$$

Since Ω appears only as $\cos \Omega z$ in both I and II , those double integrals will yield expressions which can be written as $F_{I,II}(\gamma, \omega, t_1, \Omega) + F_{I,II}(\gamma, \omega, t_1, -\Omega)$. We shall explicitly display only the first of these terms. The integral I can thus be written

$$I = - \int_0^{t_1} dt \left(\frac{1 - e^{-(\gamma+i\omega+i\Omega)(t_1-t)}}{2(\gamma+i\omega+i\Omega)} \right) = \frac{t_1}{2(\gamma+i\omega+i\Omega)} + \frac{e^{-(\gamma+i\omega+i\Omega)t_1} - 1}{2(\gamma+i\omega+i\Omega)^2}. \tag{2.35}$$

Hence

$$\operatorname{Re}\{I\} = \frac{t_1 \gamma}{2[\gamma^2 + (\omega + \Omega)^2]} + \frac{-[1 - e^{-\gamma t_1} \cos(\omega + \Omega)t_1][\gamma^2 - (\omega + \Omega)^2] - 2e^{-\gamma t_1} \sin[(\omega + \Omega)t_1]\gamma(\omega + \Omega)}{2[\gamma^2 + (\omega + \Omega)^2]^2}.$$

The same terms with Ω replaced by $-\Omega$ must be added to this expression.

We now consider II . The first integral is given by

$$A_1 = \int_0^{t_1} e^{-(\gamma+i\omega)x} \cos \Omega(t_1 - t - x) \, dx = e^{-i\Omega t} \left(\frac{-e^{-(\gamma+i\omega)t_1} + e^{i\Omega t_1}}{2(\gamma+i\omega+i\Omega)} \right) = e^{-i\Omega t} A_2, \tag{2.37}$$

where

$$A_2 = \left\{ -[\gamma(e^{-\gamma t_1} \cos \omega t_1 - \cos \Omega t_1) - (\omega + \Omega)(e^{-\gamma t_1} \sin \omega t_1 + \sin \Omega t_1)] \right. \\ \left. + i[\gamma(e^{-\gamma t_1} \sin \omega t_1 + \sin \Omega t_1) + (\omega + \Omega)(e^{-\gamma t_1} \cos \omega t_1 - \cos \Omega t_1)] \right\} \{2[\gamma^2 + (\omega + \Omega)^2]\}^{-1}. \quad (2.38)$$

Again the same terms with $\Omega \rightarrow -\Omega$ must be added to this expression.

The t integrals in I are now given by

$$A_3 = \int_0^{t_1} dt e^{(\gamma + i\omega - i\Omega)t} = \frac{e^{(\gamma + i\omega - i\Omega)t_1} - 1}{\gamma + i\omega - i\Omega} = \left\{ [\gamma(e^{\gamma t_1} \cos(\omega - \Omega)t_1 - 1) + (\omega - \Omega)(e^{\gamma t_1} \sin(\omega - \Omega)t_1)] \right. \\ \left. + i[\gamma(e^{\gamma t_1} \sin(\omega - \Omega)t_1) - (\omega - \Omega)(e^{\gamma t_1} \cos(\omega - \Omega)t_1 - 1)] \right\} [\gamma^2 + (\omega - \Omega)^2]^{-1} \quad (2.39)$$

and

$$A_4 = \int_0^{t_1} dt e^{-(\gamma + i\omega + i\Omega)t} = \left\{ [-\gamma(e^{-\gamma t_1} \cos(\omega + \Omega)t_1 - 1) + (\omega + \Omega)(e^{-\gamma t_1} \sin(\omega + \Omega)t_1)] \right. \\ \left. + i[\gamma(e^{-\gamma t_1} \sin(\omega + \Omega)t_1) + (\omega + \Omega)(e^{-\gamma t_1} \cos(\omega + \Omega)t_1 - 1)] \right\} [\gamma^2 + (\omega + \Omega)^2]^{-1}. \quad (2.40)$$

The power spectrum [Eq. (2.30)] is thus

$$G(\nu) = \frac{4\beta}{t_1} [\text{Re}\{I\} + \text{Re}\{SA_2(A_3 + A_4)\}]. \quad (2.41)$$

Here the various terms are given by Eqs. (2.34), (2.36), (2.38), (2.39), and (2.40). After some algebraic manipulations, a reduced form for $G^+(\nu)$ may be obtained:

$$\frac{G^+(\nu)}{\beta} = \frac{4\gamma}{\gamma^2 + (\omega - \Omega)^2} + \frac{8}{t_1[\gamma^2 + (\omega - \Omega)^2]P} \left(\frac{[\gamma^2 - (\omega - \Omega)^2]Q - 2\gamma(\omega - \Omega)R}{\gamma^2 + (\omega - \Omega)^2} + \frac{(\omega^2 - \Omega^2 - \gamma^2)Q + 2\gamma\omega R}{\gamma^2 + (\omega + \Omega)^2} \right), \quad (2.42a)$$

where

$$P = \cosh(2\gamma t_1) - \cos(2\omega t_1), \quad (2.42b)$$

$$Q = -0.5 \sinh 2\gamma t_1 + \sinh \gamma t_1 \cos \omega t_1 \cos \Omega t_1, \quad (2.42c)$$

$$R = \cosh \gamma t_1 \sin \omega t_1 \cos \Omega t_1 - 0.5 \sin 2\omega t_1. \quad (2.42d)$$

As necessary, all terms but the first in Eq. (2.42a) disappear if either $t_1 \rightarrow \infty$ or $\Omega \rightarrow 0$.

III. EXPERIMENTAL PROCEDURE AND DATA ANALYSIS

Rectangular platinized platinum electrodes of about 250- μm gap separation were used to apply an electric field to suspensions of 0.81- μm polystyrene spheres (Dow Chemical Co.) as shown in Fig. 2. The distilled water in which the spheres were suspended was buffered to a pH of 8.5 by 0.001 M NaHCO_3 . A 15-mW HeNe laser (Spectra Physics 124A) served as a light source. For heterodyne detection, light scattered from the cuvette walls was used as the reference beam. Light scattered from the moving particles as well as from the cuvette windows was collected at the selected angle with a photomultiplier and the photocurrent was amplified and sent to a real-time

spectrum analyzer (SAICOR SAI-52A). Spectral information is accumulated in this arrangement with nearly perfect efficiency in real time. Typical spectra are shown in Figs. 3-6 for a scattering angle of 16.4° and a 35-V/cm electric field. Integration times for these spectra were 1-2 min. The applied electric field in the solution was deduced to be rectangular to within a few percent since the measured current through the cell was rectangular to that precision. The specific methods of obtaining high electric fields and other performance characteristics of the narrow-electrode-gap arrangement will be described in a separate paper.⁹ Here we wish to describe the effects of the alternating field and the attainable resolution for such a system.

In principle, any two points on an experimental curve could be used with Eqs. (2.42) to determine γ and Ω . There is, of course, an over-all amplitude factor which adds one additional parameter to be determined.

Direct evaluation of Eqs. (2.42) for various γ and Ω shows a series of peaks at the harmonic angular frequencies $n\pi/t_1$ whose full width at half-maximum is $\Delta\omega_{1/2} = 2\gamma$. The experimental curves show peaks of fairly uniform width at those fre-

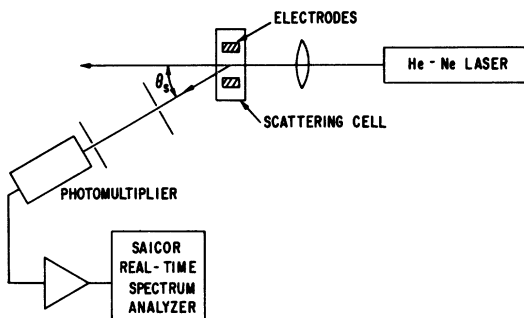


FIG. 2. Schematic diagram of the experimental arrangement. The dimensions of the cuvette are 2×10 mm², and 45 mm deep. Electrodes were immersed in the cuvette as shown. At small scattering angles the electric field was therefore nearly along the scattering vector. The high-resolution measurements were made with an electrode gap of about 250μ . The Saicor 52A spectrum analyzer (400 channels) has a resolution of 0.5 Hz for the 200-Hz full scale range used in these experiments. The laser used was a 15-mW He-Ne laser (Spectra Physics 124A).

quencies. If that width is identified with 2γ , then the ratio of any two peak heights is sufficient to determine Ω .

At any $\omega_n = n\pi/t_1$ we have, from Eqs. (2.42),

$$G^+(n) = \frac{8\beta[-0.5 \sinh 2\gamma t_1 + (-1)^n \sinh \gamma t_1 \cos \Omega t_1]}{t_1[\gamma^2 + (\omega_n - \Omega)^2][\cosh 2\gamma t_1 - 1]} \times \left(\frac{\gamma^2 - (\omega_n - \Omega)^2}{\gamma^2 + (\omega_n - \Omega)^2} + \frac{\omega_n^2 - \Omega^2 - \gamma^2}{\gamma^2 + (\omega_n + \Omega)^2} \right) + \frac{4\gamma\beta}{\gamma^2 + (\omega_n - \Omega)^2}.$$

Then $G^+(n)/G^+(n')$ can be varied as a function of Ω and fit to the experimental ratio.

This procedure was applied to a large number of experimental determinations of the electrophoretic mobility of polystyrene spheres. Here we present an analysis of the typical set of experimental results shown in Figs. 3-6. In these runs, the electric field was held constant and power

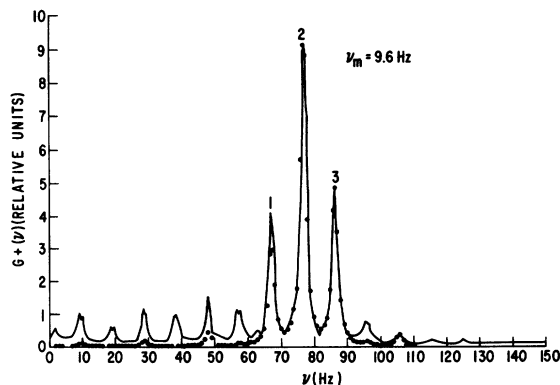


FIG. 3. Solid curve; experimental trace. Points as calculated in Sec. III.

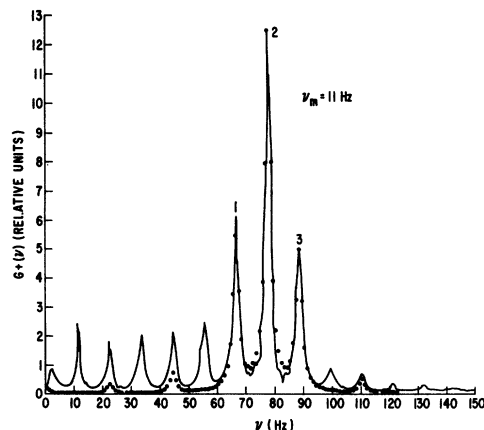


FIG. 4. Solid curve; experiment trace. Points as calculated in Sec. III.

spectra were taken for various modulation frequencies.

For each spectrum, an average peak width $\Delta\nu_{1/2} = \Delta\omega_{1/2}/2\pi = \gamma/\pi$ was determined. As may be seen from the figures and Table I, the variation about the average width was relatively small, i.e., $\pm 15\%$. Moreover, the numerical determination of the Doppler frequency $F = \Omega/2\pi$ was quite insensitive to the precise value of γ taken within these limits.

For each spectrum, F was calculated from two ratios of peak heights. The first ratio R_1 , the height of the peak labeled 1 in Figs. 3-6 divided by the height of that labeled 2, yielded F_1 . The second ratio R_2 , the height of the peak labeled 3 to that labeled 2 in each figure, yielded F_2 . As may be seen from Table I, R_2 yielded a generally more consistent set of frequencies. In general, good agreement between F_1 and F_2 was obtained for $\nu_M < F$ where ν_M , the modulation frequency, is given by $1/(2t_1)$. As ν_M increases, some inconsistencies begin to appear. These may be under-

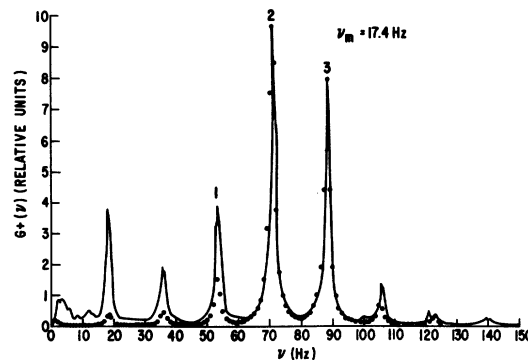


FIG. 5. Solid curve; experimental trace. Points as calculated in Sec. III.

stood by looking at the representative power spectra in the figures. The dots are calculated points. These points are normalized so as to match the experimentally obtained height at peak 2, and F is chosen so that the height at peak 3 is also matched. In general, the lower the frequency of a peak, the poorer the agreement between calculated and experimental peak height. There seems to be an extraneous source of peak strength in the low frequency regime which will be discussed in Sec. IV.

When large modulation frequencies are used, the experimental curves bear little resemblance to spectra characteristic of a single Doppler frequency. It is not possible to discern even an envelope of the harmonic peaks around the particle Doppler frequency. Thus, although the accuracy of the mobility determination is reduced in such cases, our fitting procedure then becomes particularly useful.

The spectrum features of Table I were reproduced for a variety of angles and electric field strengths, and for different electrodes. The Doppler frequencies deduced from the spectra were consistent with a single mobility value for the polystyrene spheres ($3.8 \pm 0.1 \mu/\text{sec})/(\text{V}/\text{cm})$ for the $0.82\text{-}\mu\text{m}$ spheres from Dow Chemical Co. in 0.001 M NaHCO_3 . Furthermore, for some conditions, the electrode polarization was not large and we could apply a quasistationary field ($\nu_M = 1\text{ Hz}$ or less) with some success. The mobility values deduced from the unstructured spectra which resulted from such a field compared well with the mobility values deduced from the structured spectra and verified the constant field limit of Eq. (2.42a).

IV. DISCUSSION

The agreement between the theoretical prediction and experimental observation of the spectrum

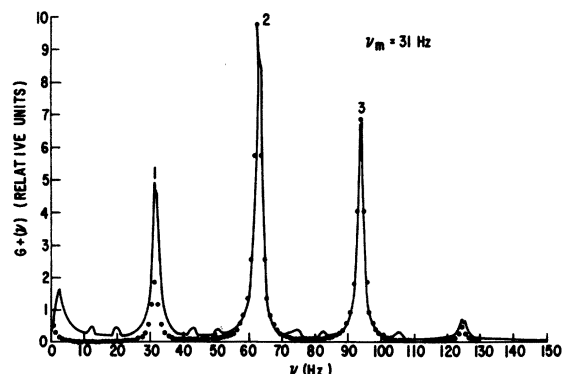


FIG. 6. Solid curve: experimental trace. Points as calculated in Sec. III.

from a suspension of polystyrene spheres is quite good. It is possible, furthermore, to pick out a central Doppler frequency even when the harmonic structure of the power spectrum shows no clear central peak. The typical results, shown in Table I, indicate that for a range of switching frequencies the precision of determination of the central Doppler frequency F from a three-point fit is better than a few percent, typically about 1 Hz out of 77 Hz. The observed Lorentzian width due to random motion is about 3 Hz. For an ideal system we may expect to split such a line to the resolution limit of the analyzer, which is 0.5 Hz in the frequency range used here. Thus the central frequency from the modulated data is determined to nearly the precision limit of the instrument. At this stage the indicated results and theoretical calculations are regarded as in excellent agreement because other precision limiting factors can cause the observed small variations from run to run. For example, either small temperature gradients or microphonics may easily cause small time varying frequency changes in the observed spectrum. Such effects exist even without the application of an electric field as is indicated by the fact that at times the Lorentzian width in zero field is slightly larger than calculated for pure diffusion for these size spheres ($\Delta\nu_{1/2} \sim 2.5\text{ Hz}$ for 16° scattering angle and $0.82\text{-}\mu\text{m}$ spheres). Finally, broadening effects due to some finite mo-

TABLE I. Typical experimental data and the results of their analysis.

ν_M (Hz)	ν_n (Hz)	$\Delta\nu$ (Hz)	$\Delta\nu_{av}$ (Hz)	$G(\nu)$ (rel)	F_1 (Hz)	F_2 (Hz)
7.8	70.2	3.0		5.75	77.74	78.33
	78.0	2.6	3.03	11.66		
	85.8	3.5		5.22		
9.6	67.2	2.1		4.11	76.73	78.26
	76.8	2.1	2.03	9.18		
	26.4	2.0		4.91		
11.0	66.0	2.5		5.81	76.78	77.15
	77.0	2.5	2.63	12.50		
	88.0	2.9		5.00		
12.0	60.0	2.6		5.68	72.58	77.81
	72.0	2.8	2.66	13.81		
	84.0	2.6		12.48		
17.4	52.2	2.4		3.90	70.86	77.47
	69.6	2.1	2.23	9.69		
	87.0	2.2		8.00		
26.0	52	3.1		5.90	76.71	74.17
	78	2.4	2.86	10.95		
	104	3.1		2.80		
31	31	2.9		4.72	63.64	74.87
	62	2.3	2.40	9.76		
	93	2.0		6.88		
39	39	3.1		7.80	72.09	70.07
	78	2.6	2.96	10.65		
	117	3.2		2.21		

bility distribution for the polystyrene spheres as well as from the fringing fields of the electrodes must inevitably limit the precision of the mobility measurement in these experiments. It should be noted that for the experimental conditions used, modulation frequencies much lower than indicated in Table I produce a broadening of the spectra due to electrode polarization effects and electrode surface reaction effects.

There is however a clear systematic shift of the deduced Doppler frequency as the modulation frequency was increased to 17 Hz and beyond. Several effects may be responsible for the errors. A small tail in the spectrum due to field inhomogeneity, a mobility distribution, or residual homodyne term can cause the harmonic peaks on the low-frequency side to be higher than for an ideal system. A "crosstalk" type of error can result and become more severe as the modulation frequency is increased. Indeed an increase of the frequency error at large modulation frequency was observed as the spectrum tail was artificially increased by geometrical manipulation, i.e., by collecting more fringing field and inhomogeneity contributions to the light scattering signal. Nevertheless, from Table I we see that a central frequency can be discerned to within about 6% of the true Doppler frequency even at the higher modulation frequencies.

The errors in determining the central Doppler frequency at high modulation frequencies represent a practical limit to the upper value of the switching frequency that may be profitably applied to the system under study. Possibly, with appro-

prate experimental modifications these errors may become less severe. The response time τ_R of the particle is not limiting since¹⁰

$$\tau_R \cong m/3\pi\eta d \cong 10^{-6} \text{ sec} \ll V_M^{-1}.$$

Here m is the particle's mass, d is its diameter, and η is the viscosity. A fundamental upper limit does exist, however. If particle motion is reversed before a significant phase shift develops in the scattered light field then the photocurrent spectrum will not reveal any information on the particle velocity. In terms of the equations above, the harmonic peaks will become vanishingly small—one requires at least two peak amplitudes to determine particle velocity.

Another important consideration is the resolution of multicomponent systems. If a number of sharp mobility components are present, then the power spectrum must be fit to a finite sum of terms of the type given in Eqs. (2.42) each with a different γ and Ω . If the mobility distributions are broad compared to the modulation frequencies then of course the envelope of the harmonic spectra peaks would approximate the true velocity distributions in the electric field.

We have demonstrated that the light-scattering spectra from particles in a square-wave electric field are clearly interpretable and can lead to high-resolution measurements of electrophoretic mobilities. This result should increase the usefulness, accuracy, and range of applicability of electrophoretic mobility measurements by the technique of laser doppler spectroscopy.

¹G. B. Benedek, in *Polarisation, Matière, et Rayonnement* (Presses Universitaires de France, Paris, 1969), p. 49 (volume jubilaire en l'honneur d'Alfred Kastler).

²H. Z. Cummins and H. L. Swinney, in *Progress in Optics* (North-Holland, Amsterdam, 1970), Vol. 8, p. 135.

³R. Foord *et al.*, *Nature* **227**, 242 (1970).

⁴B. R. Ware and W. H. Flygare, *Chem. Phys. Lett.* **12**, 81 (1971).

⁵E. E. Uzgiris, *Opt. Commun.* **6**, 55 (1972).

⁶B. R. Ware and W. H. Flygare, *J. Colloid Interface Sci.*

39, 670 (1972).

⁷See, for example, *Electrophoresis, Theory, Methods, and Applications*, edited by M. Bier (Academic, New York, 1959), Vol. I.

⁸J. S. Bendat, *Principles and Applications of Random Noise Theory* (Wiley, New York, 1958).

⁹E. E. Uzgiris (unpublished).

¹⁰*Colloid Science*, edited by H. R. Kruyt (Elsevier, New York, 1952).